Polymer 49 (2008) 5541–5548

Contents lists available at ScienceDirect

Polymer

journal homepage: www.elsevier.com/locate/polymer

Radiation tolerance in polymeric dielectrics by small-molecule doping, Part I: Dopant uptake as a function of temperature, time, and chemistry

Robert J. Klein [a], Shannon M. Cole [b], Michael E. Belcher [b], John L. Schroeder [a], Phillip J. Cole [c,**], Joseph L. Lenhart [a,d,*]

[a] Organic Materials Department (1821), Sandia National Laboratories, Albuquerque, NM 87185, United States
[b] Organic Materials Department (2453), Sandia National Laboratories, Albuquerque, NM 87185, United States
[c] NNSA Satellite Programs (5732), Sandia National Laboratories, Albuquerque, NM 87185, United States
[d] US Army Research Laboratory, Weapons and Materials Research Directorate, Aberdeen Proving Ground, MD 21005-5069, USA

ARTICLE INFO

Article history:
Received 24 June 2008
Received in revised form 27 August 2008
Accepted 28 August 2008
Available online 18 September 2008

Keywords:
Radiation
Polymer
Conductivity

ABSTRACT

The doping of Mylar® film (composed of semi-crystalline poly(ethylene terephthalate)) with small-molecule electron traps results in a high-quality dielectric film with excellent radiation tolerance. This paper, the first of two, investigates the doping process as small molecules are implanted into the film from a solution of ethylene glycol over time. A series of fluorenone-based dopants are investigated, functionalized by nitro or cyano groups. The concentration of dopant in the Mylar® is a strong function of time, temperature, and solution concentration. Doping is ineffective below the glass transition temperature of the polymer. The chemical functionality of the dopant had a strong effect on the doping process, with additional nitro or cyano groups leading to enhanced film concentrations.

1. Introduction

Certain applications require high-quality organic materials that can resist the deteriorating effects of continual or intermittent ionizing radiation. However, the combination of good electrical performance and high radiation tolerance in polymers is not commercially available. One route to such films is to dope commercial dielectric films with small molecules that can improve radiation tolerance. The process of doping such films varies dramatically depending on the dopant chemistry and doping conditions, and these changes must be well-understood to achieve the desired dopant concentration coincident with no degradation to the film properties. There exist a large number of dopants that all provide excellent radiation tolerance, but each exhibits unique doping behavior.

1.1. Radiation hardening

Radiation-tolerant polymers may be used in applications such as energy storage materials, protective coatings, underfills, or encapsulants. When ionizing radiation interacts with a polymeric material, whether the radiation consists of X-rays, γ-rays, protons, or high-energy electrons, electron–hole pairs are formed that lead to electrical conductivity [1,2]. This radiation-induced conductivity (RIC) severely limits the insulating capability of polymeric dielectrics used in ionizing environments. The physics of RIC in polymers, including carrier creation and carrier transport, has been extensively studied from the fundamental perspective of electronic processes occurring in disordered materials [2–7]. Incident radiation interacts with sites in the polymer to create electron–hole pairs, which may separate into mobile carriers or recombine. The electrons and holes move through the material by hopping between defect sites (polymers typically do not manifest a continuous conduction band) with different mobilities for the electrons and holes as determined by the material chemistry and morphology. In most insulating polymers, holes are more mobile than electrons [3,8], but due to a longer electron lifetime under electric fields, electrons dominate the RIC response [2,9]. As a function of radiation dose, RIC in polymers increases as a power law with an exponent between about 0.5 and 1. Conductive carrier transport and the collection of carriers by traps depend heavily on polymer chemistry, polymer morphology, and polymer relaxation dynamics, and currently no model exists that can account for RIC behavior across all undoped polymers, although the Rose–Fowler–Vaisberg model is often used for simple polymers [3,4]. If dopants are present, dopant chemistry (such as the number and strength of

* Corresponding author. US Army Research Laboratory, Weapons and Materials Research Directorate, Aberdeen Proving Ground, MD 21005-5069, USA. Tel.: +1 410 306 1940; fax: +1 410 306 0676.
** Corresponding author. Tel.: +1 202 586 1207; fax: +1 505 284 1485.
E-mail addresses: pjcole@sandia.gov (P.J. Cole), joseph.lenhart1@arl.army.mil (J.L. Lenhart).

0032-3861/$ – see front matter © 2008 Published by Elsevier Ltd.
doi:10.1016/j.polymer.2008.08.067

electron-withdrawing groups on the small molecule) further complicates RIC behavior.

Two solutions have been engineered to prevent radiation from disabling the polymeric dielectric: shielding with high-Z elements [10] or doping with electron or hole traps [2]. Shielding can be effective but requires bulky and heavy protective layers, detracting from the effort towards small and light components. Doping with electron or hole traps for the reduction of RIC has been studied and developed for a few select chemistries – namely, poly(ethylene terephthalate) and poly(vinylidine fluoride) doped with trinitrofluorenone by Kurtz et al. [2,11] – but little work has been done to extend the doping method to a large number of polymers, dopants, and processing conditions, and even less to understand the effect of chemistry on the reduction of RIC.

Recent papers [12,13] have discussed the effectiveness of a variety of electron-trapping dopants in reducing RIC in polymeric materials. The small-molecule trinitrofluorenone (TNF) reduces RIC by 98% when used at appropriate concentrations to dope poly(ethylene terephthalate) (PET), measured while radiated at 30 rad/s (Si). Other small-molecule electron traps, such as tetracyanoquinodimethane (TCQM), nitroacenaphthene (NAN), and dinitrofluorenone (DNF), reduce RIC under similar conditions by 89–98% [12]. Table 1 provides characteristic values for RIC in the presence of dopants: RIC reduction is the motivation for this investigation of the doping process.

1.2. Small-molecule doping of polymers

Diffusion of small molecules in polymers has been studied previously for a huge range of industrial and commercial applications, including plasticization of glassy polymers [14], ion transport in battery membranes [15,16], acid diffusion through photoresist [17], gas diffusion through membranes [18,19], hydrocarbon liquid loss from rubber tubing [20], drug release and agricultural agent release from inert polymers [21], drying of paints [22], and dyeing of fabrics [23], among others. Diffusion through polymers in the most basic sense is driven by a concentration gradient and assisted by Brownian motion [24], which in polymers can include local rotation and long-range cooperative motion [25]. Fick's second law governs concentration diffusion within the membrane over time. Complicating factors for applications include a diffusivity dependence on the local concentration of dopant, swelling of the film by the carrier solvent, and porosity on the micron scale [1,26,27].

Diffusion above T_g is generally viewed as consisting of a molecular dopant being embedded into the fluctuating free volume within the polymer, where the local pockets of free volume continuously shift due to the fluid state of nearby polymer chains [28]. The dopant may then hop between pockets of free volume by virtue of its kinetic energy, although the frequently observed correlation between diffusion and polymer segmental motion indicates some level of coupling [25,28]. The fluidity of the pockets of free volume greatly lowers the energetic barrier for hopping, and below T_g where the amorphous chains can neither assist dopant motion directly nor shift to accommodate the dopants, there is a discontinuous drop in the diffusivity. In semi-crystalline polymers, the crystalline regions are generally treated as completely impermeable to small-molecule diffusion (exhibiting orders of magnitude lower diffusivities), and so dopants must follow a nonlinear path through the amorphous regions.

The thermodynamic driving force for diffusion of small molecules from solvent (phase I) to polymer (phase II) is the chemical potential difference for the dopant in the respective phases [29,30]. Depending on the specific interactions between the dopant (solute) and the two phases, partitioning of the dopant between solvent and polymer may lead to higher or lower concentrations in the polymer. Specific expressions for the equilibrium at constant temperature and pressure rely on a balance of the fugacities and therefore the activity coefficients in the two phases; such expressions will be covered in more detail in paper II. At this point it is important to specify that most experimental investigations of solute partitioning obtain a linear relationship between the concentrations in phase I and phase II [31]. This is especially true at low concentrations, when the solute is far from saturating phase II and represents Henry's law, but at higher concentrations, deviations from linearity may occur due to, e.g., filling of the free volume within phase II. In this case the solute concentration in phase II often reaches a plateau, and may be treated as a pseudo-Langmuir isotherm. Langmuir-like plateaus have been observed in dye transport into porous beads by Weisz et al. [32–34] and gas sorption in glassy polymers by Vieth et al. [18,35].

Table 1
Radiation-induced conductivity (RIC) of PET doped by electron traps [12]

Dopant	Conc. of dopant (mol/m^3) in PET	RIC (pA)	RIC reduction (%)
None	0	204	0
TCQM	1.1	29	86
NAN	14	14	93
TNF	50	3.0	98
DNF	25	3.7	98
NF	21	8.0	96
CF	70	47	77

1.3. Doping with electron traps for reduced RIC

Due to the photo-activity and electron-withdrawing ability of fluorenones, doping with TNF has been utilized in many contexts. Lardon et al. [36] introduced and Melz [37] expanded the study of poly(*N*-vinyl carbazole) (PVK) complexed with TNF, examining photogeneration efficiency under visible light as a function of applied electric field in the context of Onsager theory. However, the doping was performed by simply dissolving TNF and PVK in a co-solvent and evaporating the solvent. Hughes [38] performed similar studies of the same material to examine carrier recombination kinetics. In 1983 Kurtz et al. [1] extended the concept of TNF-based photogeneration to obtain for the first time TNF-doped PET that exhibited reduced RIC while exposed to X-rays. Benzyl alcohol, which swells PET, was used as the carrier solvent and doping was performed at room temperature. However, significant swelling of the PET degrades film quality and dielectric breakdown strength, and ethylene glycol was selected as a viable solvent with minimal swelling effects.

Here we consider a series of fluorenone-based dopants – TNF, DNF, nitrofluorenone (NF), cyanofluorenone (CF), and fluorenone (F) – and nitropyrene (NP) impregnating PET from a solution of ethylene glycol (EG) under a wide range of experimental conditions. This paper, the first of two, will discuss experimental preparation and characterization methods, and present data that describe the physics of the doping process across temperature, concentration, and dopant chemistry. The second paper in the series will utilize a physical model and fit the data to obtain parameters describing the kinetics and thermodynamics of doping specific to each dopant chemistry.

2. Experimental

2.1. Materials

2-Nitrofluorenone (NF, 99%), 2,7-dinitro-9-fluorenone (DNF, 97%), 2,5,7-trinitro-9-fluorenone (TNF, 99%, Sandia National Laboratories), 9-fluorononone (F, 99%), 4-cyano-9-fluorononone (CF, 99.5%),

1-nitropyrene (NP, 99%), isopropanol (99.9%), acetone (99.5%), toluene (99.8%, Acros), and ethylene glycol (EG, electronic grade, Air Products) were obtained from Fisher Scientific unless otherwise noted. Mylar® C capacitor-grade poly(ethylene terephthalate) (PET) film of 12.9 μm in thickness was obtained from DuPont. Chemical structures of the dopants and polymer are given in Fig. 1.

2.2. Film preparation and characterization

PET films, with surfaces cleaned by wiping with cloth soaked in isopropanol, were held in heated EG solutions prepared with the proper concentration of small-molecule dopant for specified times. Solution temperature T and solution concentration C_S were carefully controlled over the duration of the doping time t (Fig. 2). The films were then removed, rinsed in isopropanol, acetone, and toluene, and annealed under vacuum at 82 °C for at least 12 h.

For each dopant, concentration calibration curves were established by ultraviolet–visible (UV–vis) spectroscopy (PerkinElmer, Lambda 950) in transmission mode using solutions of known concentrations. A characteristic band for each dopant was selected and the absorbance of this band used to calculate concentrations by Beer's law (Fig. 3). All absorbance calibration curves were linear and intersected the origin, as seen in Fig. 3 for TNF. Concentrations in the films were then determined from UV–vis transmission mode by subtracting a spectrum representing PET and then applying the appropriate calibration curve (see Fig. 4 for an example). The absorption cross sections σ were calculated considering the path length of the calibration solutions or the film thickness. Values of σ were found to be independent of solvent, signifying that UV–vis absorption by the dopant scaled with concentration in the same manner for different environments. Table 2 provides values for each dopant of the molar absorptivity ε (slope of the calibration curves), obtained as absorbance over concentration, as well as the wavelength λ where absorption was evaluated.

Dynamic mechanical analysis (DMA) and differential scanning calorimetry (DSC) were used to characterize the glass transition.

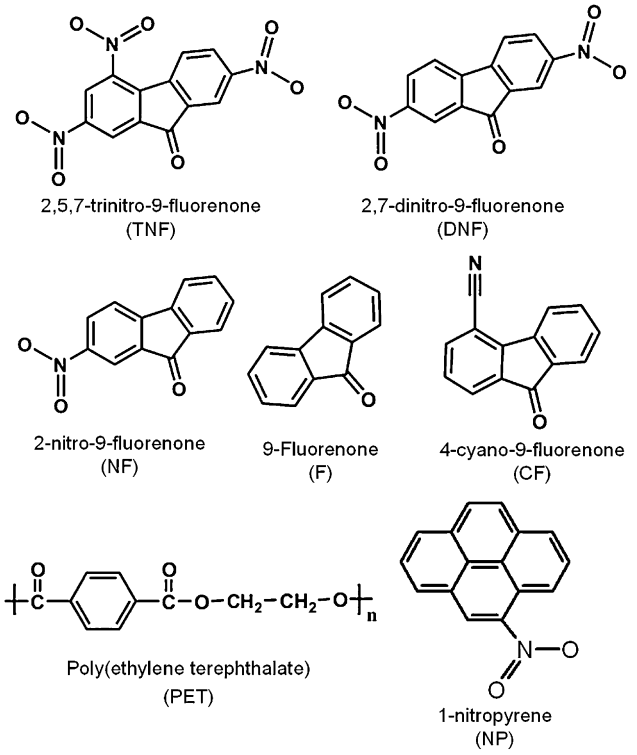

Fig. 1. Chemical structures of the dopants and polymer used in this study.

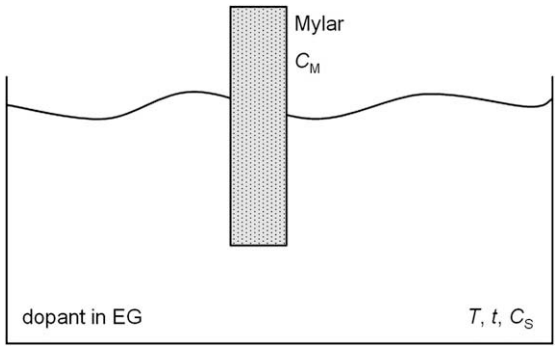

Fig. 2. Schematic of the dipping process used to impregnate PET with dopant. Independent variables include temperature T, doping time t, and dopant concentration in the solvent C_S, all of which determine the final dopant concentration in the PET film (C_m).

DMA utilized a TA Q800 with conditions of 1 Hz, ~0.1% strain, 50 mL/min flow of N_2, and a positive temperature ramp of 2 °C/min. DSC utilized a TA Q100 under a positive temperature ramp of 10 °C/min and 50 mL/min N_2 flow. DSC was the primary method to

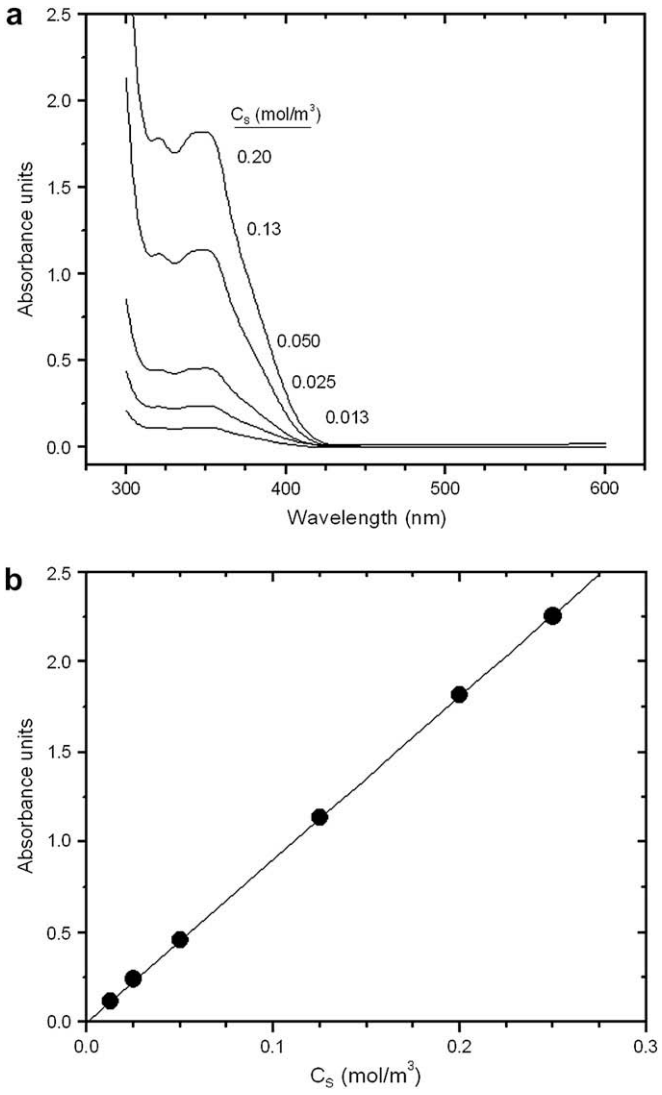

Fig. 3. (a) UV–vis absorption spectra for TNF in ethylene glycol solution and (b) calibration curve for TNF obtained from the magnitude of the UV–vis curves at 345 nm. The error in the absorbance at a particular wavelength is ca. ±3%, as determined from multiple samples.

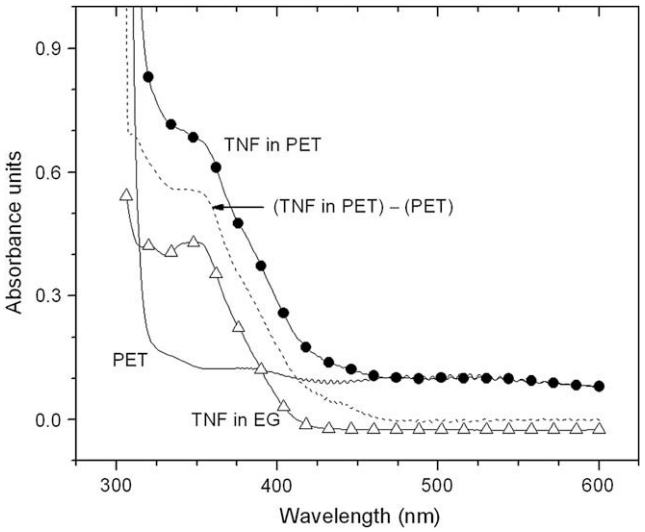

Fig. 4. UV–vis absorption spectra for (1) TNF-doped PET, (2) undoped PET, the difference between (1) and (2), and TNF in EG. The UV–vis absorbance of pure EG is essentially zero. All other dopants and conditions yielded similar spectra. The error in the absorbance at a particular wavelength is ca. ±3%, as determined from multiple samples.

determine T_g, and because of the weak signal, DMA was used as confirmation of the glass transition temperature.

The few films exposed to ultraviolet–ozone (UV–O) were done so using atmospheric oxygen and a high-intensity mercury lamp (Jelight, UVO-Cleaner) for 2 min. The mercury lamp output was 28 W/cm^2 at 254 nm, the distance to the sample was approximately 4 cm, and the relative humidity in the chamber was 10 ± 5%.

3. Results and discussion

Large data sets of concentrations have been compiled for fluorenone-based dopants impregnating PET at various conditions, allowing a thorough analysis of the doping mechanisms. Fig. 5a shows the UV–vis absorbance spectra for TNF-doped PET as a function of the doping temperature, for 20 h doping times. Using calibration curves obtained from solution standards, the corresponding TNF film concentrations are collected in Fig. 5b. The first essential point illustrated by these plots is that significant impregnation does not occur below the polymer glass transition temperature T_g. After 20 h at 40, 50, and 60 °C doping the absorbance spectra for the doped PET were indistinguishable from that of neat PET, denoting insignificant TNF uptake. At 75 °C and above, a measurable amount of TNF was observed, with substantial increases at higher doping temperatures.

Depending on material history, the extent and type of crystallinity in PET may vary widely, with large influence on the T_g. Values of 61, 81, and 125 °C were reported for amorphous (quenched), unoriented semi-crystalline (slow-cooled), and highly crystalline (cold-drawn) PET, respectively [39,40]. For the films in this study,

Table 2
UV–vis molar absorptivities ε and wavelength λ where absorption was evaluated for each dopant

Dopant	ε (a.u.-L/mol)	λ (nm)
TNF	9052	345
DNF	4362	374
NF	1936	374
CF	318.8	374
F	255.9	377

a.u. represents UV–vis transmission absorbance units.

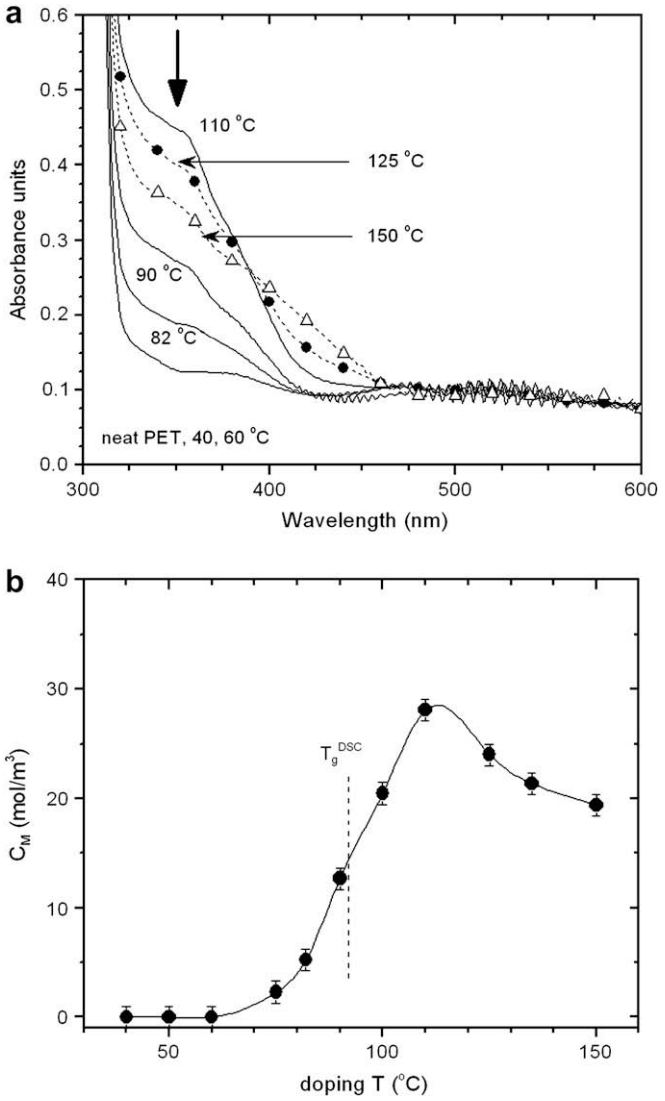

Fig. 5. (a) UV–vis spectra for TNF-doped PET after 20 h of doping, at temperatures ranging from 40 to 150 °C. Neat PET overlaps with 40 and 60 °C. The vertical arrow denotes 345 nm, the wavelength where absorbance values were evaluated for TNF. (b) PET concentrations as a function of doping temperature for TNF. Errors are estimated and the line is drawn to guide the eyes. The T_g^{DSC} of PET is 92 ± 1 °C.

PET in the Mylar® capacitor-grade film is biaxially oriented to a crystallinity of approximately 39% (calculated in detail in paper II). Fig. 6 provides results for the T_g of this material, utilizing the techniques of both differential scanning calorimetry (DSC) and dynamical mechanical analysis (DMA). From the midpoint of the DSC inflection, the T_g is ~92 °C; from the peak in the DMA loss tangent, the T_g is ~113 °C. (Note that heavy doping of Mylar® leads to minor changes in T_g.) Differences between values of T_g measured by different techniques are common, because the T_g^{DSC} is a strong function of heating rate and the DMA T_g is a strong function of frequency. In addition, the glass transition of this material is extremely broad. However, the data from both techniques indicate an initial softening point between 70 and 75 °C. This information indicates that the transition in doping behavior near 75 °C (Fig. 5b) is due to the onset of the T_g. Abrupt changes in transport behavior in polymers often occur near the glass transition temperature, below which the matrix is glassy and above which segmental motion is active. As noted previously, transport in the glassy phase involves hopping between disordered vacancies, representing frozen-in free volume, whereas above T_g it is possible for free volume to fluidly

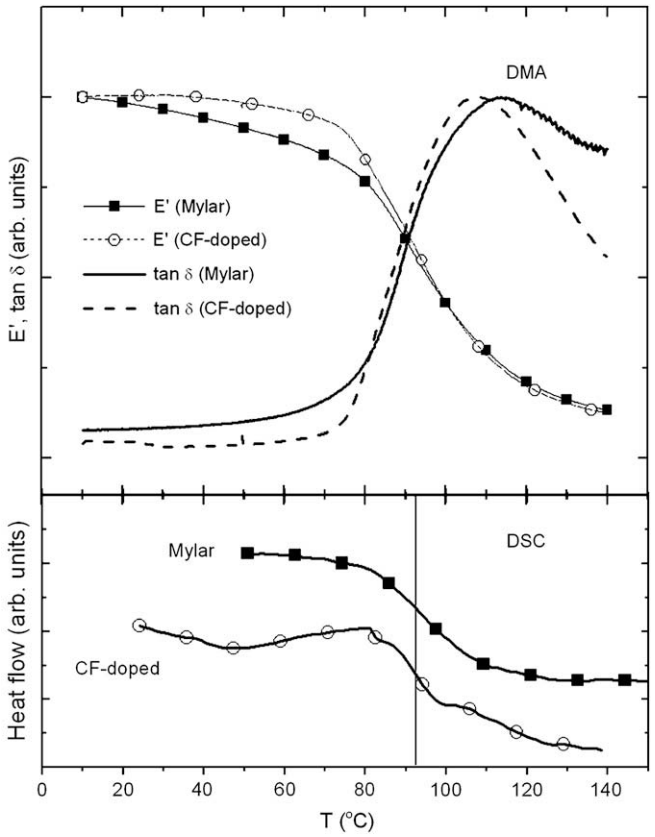

Fig. 6. Thermal scans of Mylar® and heavily CF-doped (~450 mol/m^3) Mylar® illustrating T_g, using dynamical mechanical analysis (DMA) and differential scanning calorimetry (DSC). DMA data were collected at 1 Hz, 2 °C/min, and 0.1% strain, and the DSC was ramped at 10 °C/min. The vertical dashed line indicates the inflection point of the DSC transition, taken as the T_g^{DSC}.

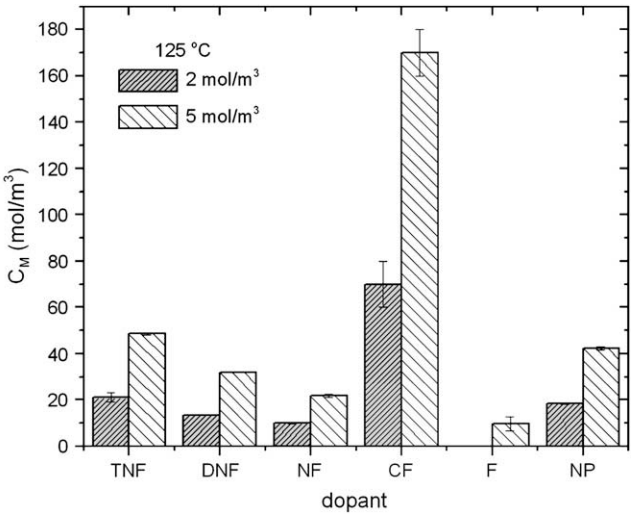

Fig. 7. Film dopant concentration C_m for various dopants, at 2 and 5 mol/m^3 solution concentration C_S, after doping for at least 4 h at 125 °C. The point for F was obtained by dividing the C_m obtained at $C_S = 20$ mol/m^3 by four. Error bars indicate standard deviations.

accommodate hopping molecules as well as for segmental, long-range polymer motion to assist solute transport [25,28,41]. Another very important result demonstrated by Fig. 6 is that a very highly doped film has a T_g essentially unchanged from the undoped material. This indicates that addition of the dopant to the film will not change the diffusivity over time, thus avoiding auto-accelerating effects that can be seen when plasticizers are added to polymers [26].

The importance of T_g points to diffusion as playing a major role in the doping process. Typical analyses of small-molecule incorporation use a simple model of diffusion to great success [24,26]. It is critical to note that the initial increase in C_m in Fig. 5b with increasing doping temperature is due to the exponential increase in diffusivity with increasing temperature. Therefore at all temperatures below 110 °C, dopant concentrations are diffusion-limited and are not at equilibrium. Once the temperature exceeds T_g by a critical amount, C_m is not diffusion-limited and reaches equilibrium in the sampled time scale. (Data sets for 100 °C evaluate concentration at long enough times to ensure that equilibrium values are obtained.) Diffusivity D for small molecules in polymers increases with an Arrhenius temperature dependence below T_g and an Arrhenius or Vogel–Fulcher–Tammann dependence above T_g [25,26,41,42]. Therefore, the decrease in C_m at temperatures above 110 °C (Fig. 5) indicates that the equilibrium partitioning of dopant decreases with increasing temperature.

Fig. 7 displays dopant concentrations in PET for the various fluorenone molecules, for solution concentrations of dopant in EG of 2 and 5 mol/m^3 and a doping temperature of 125 °C. Long doping times, at least 4 h, were utilized to ensure equilibrium dopant concentrations were reached in the films. Dopant concentration in the films is a strong function of dopant chemistry. Each additional nitro group (NO_2) on the small molecule enhances the final C_m considerably, seen in the trend of dopant concentrations TNF > DNF > NF > F. Fluorenone, which contains only a carbonyl group pendant to the three ring core, doped to very small concentrations relative to the other dopant molecules (Fig. 7). (Note that due the small molar absorptivity for F, a small change in absorbance leads to a large calculated change in concentration. Therefore the concentration of F at 5 mol/m^3 was estimated via linear extrapolation from data at 20 mol/m^3, where C_m could be measured more precisely.) The addition of a cyano group in the form of CF leads to surprisingly high dopant concentrations, about five times that of TNF. It is unclear exactly why the CF dopes so strongly; there may be a strong interaction between the cyano group and the Mylar®, or the CF may be more insoluble in the EG solvent than the nitro-containing dopants. The former point is partially negated by the fact that TCQM, which has four cyano groups, dopes poorly [12]. Further investigation of CF is warranted by these interesting results. Doping was also attempted with carboxylic acid fluorenone and aminofluorenone, and neither of these small molecules resulted in detectable levels of C_m, reinforcing the impact of specific interactions [43] between dopant, EG, and Mylar®. As will be discussed in paper II, these specific interactions have an impact both on the kinetics of diffusion and on the thermodynamics of partitioning.

Another interesting point observed from Fig. 7 is that the dopant concentrations in the films are substantially higher than those in the bulk doping solutions. As mentioned in Section 1, this indicates a significant concentrating effect of dopant within the Mylar® due to the chemical potential driving force. Quantitative analysis of these rate and equilibrium constants will be covered in the second paper on this topic.

For the following discussion we will denote the concentration of dopant in the film as C_m and the concentration of dopant in the solution as C_S. Values of C_m are unique for each dopant, time, temperature, and C_S. Fig. 8 shows the development of C_m with time in the doping solution. All five dopants exhibit similar behavior, a quick rise followed by a plateau as the concentration equilibrates. As temperature increases, the rise occurs more quickly since $D \sim \exp(-1/T)$. As seen in Fig. 9, the plateau, or

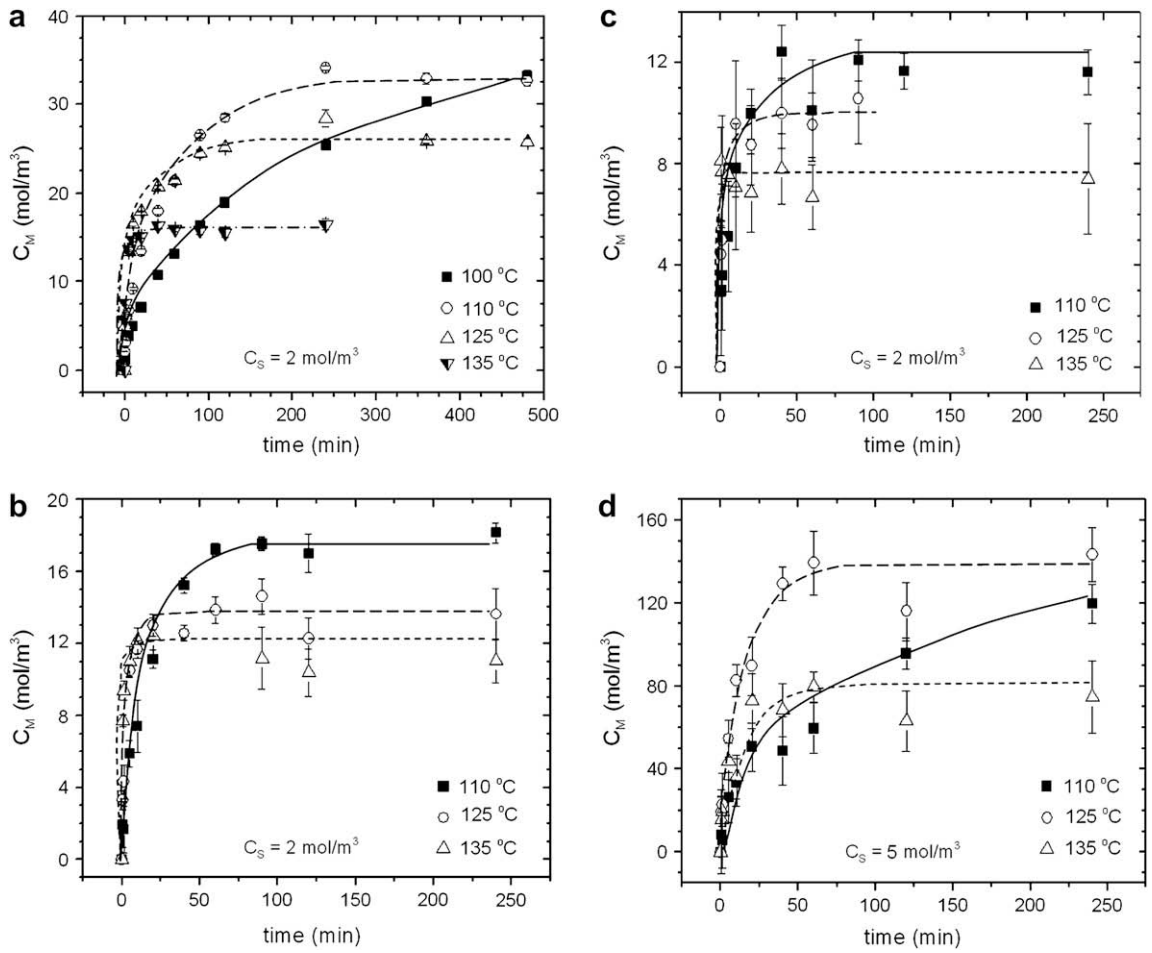

Fig. 8. Film concentration C_m as a function of time for various temperatures, for (a) TNF, (b) DNF, (c) NF, and (d) CF. Error bars indicate standard deviations, and lines are drawn to guide eyes.

equilibrium, film concentration can then be plotted as a function of solution concentration for each temperature. Data follow linear fits extremely well, and the slopes are equal to the partition coefficients K.

In a previous publication [12] we stated that the solvent–Mylar® interface played an important role in the doping process, and hypothesized that an absorption–diffusion process controlled the dopant uptake. Several initial experimental observations appeared consistent with adsorption: enhanced dopant concentration in the Mylar® relative to the doping solution, a decrease in the equilibrium dopant uptake with increasing temperature, and a complicated dependence of dopant uptake on the solvent solubility parameter. However, these observations do not prove that dopant adsorption on the film surface plays a role in dopant transport. The experiment [12] that appeared to specifically substantiate adsorption was the impact of UV–O treatment on overall dopant concentration: after treating the Mylar® surface with UV–O, equilibrium dopant concentrations increased measurably (~10%). The experiments performed in this paper, however, are not consistent with the hypothesis of adsorption playing a major role in dopant transport. First, the relationship between C_m and C_S for NP remains linear even to extremely high values of C_m (Fig. 9f); if adsorption was active then curvature in the adsorption isotherm would be observed due to surface site saturation and packing constraints at the interface. Second, further experiments on the impact of UV–ozone on the surface showed small or no increases (Table 3), contrary to our previous work. The experimental differences leading to conflicting data between this and the previous publication [12] are not clear, as we did not characterize the specific changes in surface chemistry. The impact of UV–O is undoubtedly small, as a recent publication [44] showed that UV–O treatment of polystyrene films resulted in only ~10 atomic% implantation of oxygen at the surface. It is possible that a higher humidity during UV–O treatment in the previous report [12] could have resulted in a higher oxygen implantation. Ultimately, we have no conclusive evidence that the solvent–polymer interface plays a major role in dopant uptake, and therefore the data analysis will proceed by accounting for chemical potential differences as the driving force for dopant transport from solvent to polymer, and surface adsorption will be neglected.

Several complications of the diffusion process that are commonly observed in other systems are avoided here. Since the dopants here are present in low concentrations and also do not act as plasticizers for PET, there is no self-catalyzed diffusion (demonstrated by Fig. 6), and $C_m(t)$ is represented by two simple regions of growth and plateau. Another frequent occurrence is for the carrier solvent to swell the polymer thereby increasing the diffusion rate by orders of magnitude, as seen in the initial doping work by Kurtz using benzyl alcohol [1]. In this study EG dissolves the dopants but has virtually no swelling effect on PET. Additionally, there is no porosity in the PET film that would complicate the sorption process: pores are often found in natural materials [27] or purposely added to gel-based systems to enhance diffusion [15].

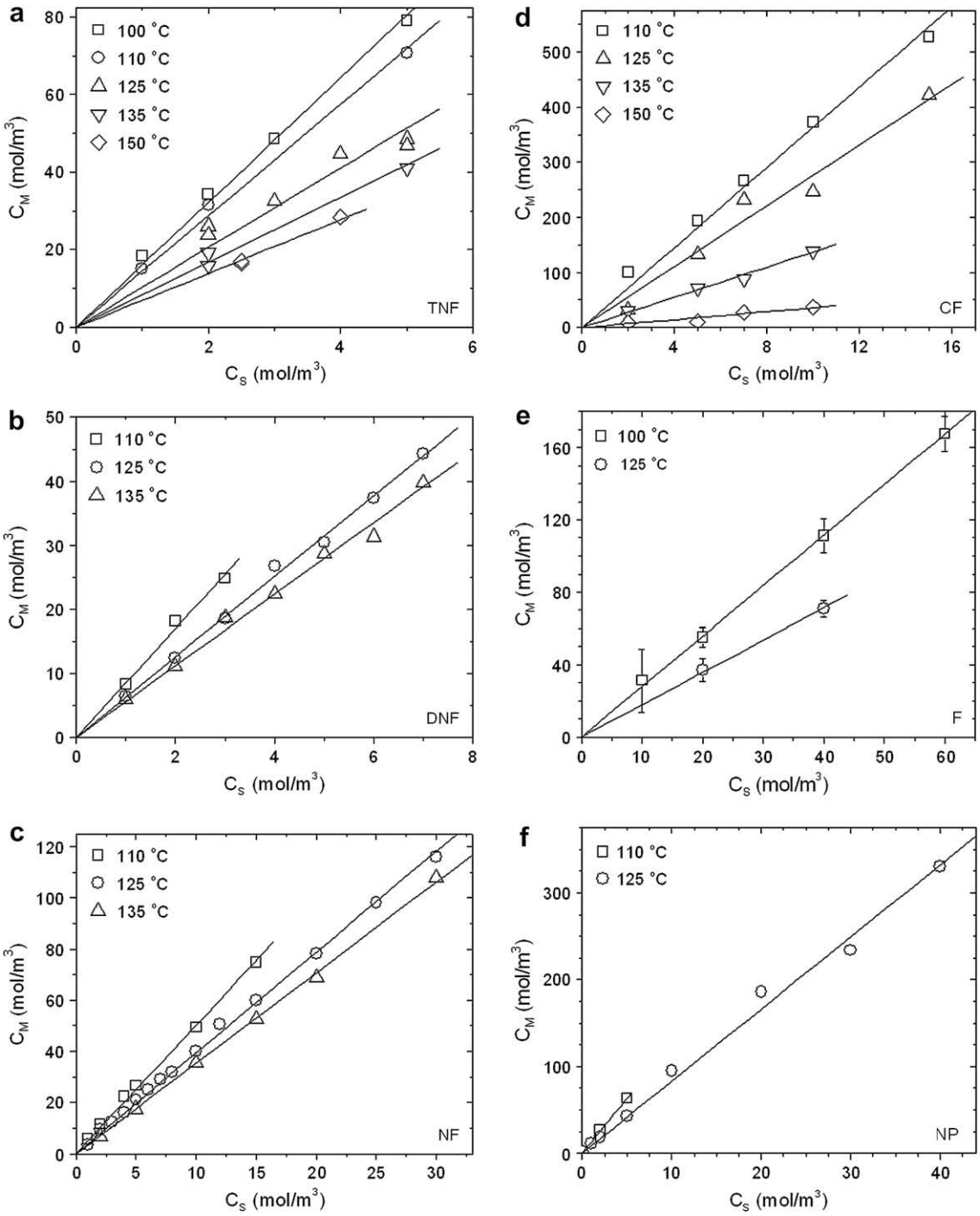

Fig. 9. Film concentration C_m as a function of solution concentration C_S doped at various temperatures for (a) TNF, (b) DNF, (c) NF, (d) CF, (e) F, and (f) NP. Lines are best fits that intersect the origin. If not shown, standard deviations are smaller than the size of the data points.

Finally, it is important to note that the presence of specific functional groups does not uniquely determine equilibrium concentration. Although CF was concentrated in the Mylar® film more strongly than any of the nitrofluorenones, indicating that the cyano group is the primary cause of such a concentrating effect, similarly large concentrations were not found for TCQM, which contains four cyano groups. Additionally, doping with NP resulted in significantly higher values of C_m than doping with NF (Fig. 7). There must therefore be a "whole molecule" effect whereby, e.g., the interactions between the cyano group and the bulk film or the solvent are enhanced by the adjacent unsaturated rings. Dipole moment is not descriptive of this effect, as the addition of adjacent double bonds does not enhance the dipole moment [45] in cyanoethylene (3.87 Debye) versus cyanoethane (4.02 Debye).

4. Summary

Doping of PET films with small-molecule electron traps has proven successful at reducing the film conductivity in a radiation environment. However, little was previously known about the process of doping PET with these small molecules. Therefore, the

Table 3
Effect of UV–O treatment on final dopant concentrations C_m for several conditions

Dopant	UV–O treated?	T (°C)	C_S (mol/m^3)	C_m (mol/m^3)
NP	No	125	1	10.8 ± 0.1
	Yes	125	1	11.1 ± 0.3
	No	125	10	93.3 ± 3.9
	Yes	125	10	96.0 ± 2.6
DNF	No	125	5	31.0 ± 0.2
	Yes	125	5	31.9 ± 0.5
	No	135	5	26.8 ± 0.9
	Yes	135	5	28.1 ± 0.3

Values for C_m were taken well into the plateau region.

doping of PET films (Mylar®) from solution with five electron-trapping fluorenones and nitropyrene was investigated over a range of solvent dopant concentrations, temperatures, and times. Doping was shown to be ineffective below the T_g of PET due to diffusion-limited behavior, and therefore doping temperatures were selected between 100 and 150 °C. The effectiveness of doping increased with the number of nitro or cyano groups per molecule, with the equilibrium film concentration exhibiting the following trend: CF > NP > TNF > DNF > NF > F. The time and temperature behavior of C_m was found to be a consequence of chemical gradient-driven diffusion, whereby dopant is selectively concentrated in the film on the basis of partition coefficients that are specific to chemistry. All dopants exhibited similar time behavior of film dopant concentration C_m, with a region of rapid increase and a plateau region. With increasing temperature above 100 °C, C_m reached a plateau more quickly due to increasing diffusivity D, but the C_m plateau values decreased with increasing temperature due to changes in the partition coefficients.

Modifying the Mylar® surface with UV–ozone did not lead to significant changes in plateau concentrations, and the relationship between C_m and C_S remained linear even at high concentrations, indicating that surface adsorption does not play a major role in the doping process. Relative to sorption of small molecules in other polymers, the doping of PET is simplified by the lack of a plasticization effect, insignificant swelling of the polymer by the solvent, and no porosity on the film surface.

The basic steps involved in doping commercial films for radiation tolerance have been established, providing an inexpensive route to produce high-quality dielectric films that can be exposed to high radiation environments while retaining their dielectric properties. With the understanding of the doping mechanism comes the ability to analyze the results in the context of a physical model. The second paper in this series will fit the time–temperature C_m data sets with a physical model to obtain values of diffusivity D and partition coefficient K as a function of temperature and dopant chemistry.

Acknowledgements

Sandia is a multiprogram laboratory operated by Sandia Corporation, a Lockheed Martin Company, for the United States Department of Energy's National Nuclear Security Administration under contract DE-AC04-94AL85000. Thanks to Mark Stavig for his assistance with the DSC and DMA.

References

[1] Kurtz SR, Arnold C, Hughes RC. Applied Physics Letters 1983;43:1132.
[2] Kurtz SR, Arnold JC. Journal of Applied Physics 1985;57:2532.
[3] Khatipov SA. High Energy Chemistry 2001;35:291.
[4] Tyutnev AP, Saenko VS, Smirnov IA, Pozhidaev ED. High Energy Chemistry 2006;40:319.
[5] Zhutayeva YR, Khatipov SA. Nuclear Instruments and Methods in Physics Research Section B: Beam Interactions with Materials and Atoms 1999;151:372.
[6] Faria RM, Gross B, Filho RG. Journal of Applied Physics 1987;62:1420.
[7] Yang GM, Sessler GM. IEEE Transactions on Electrical Insulation 1992;27:843.
[8] Hayashi K, Yoshino K, Inuishi Y. Japanese Journal of Applied Physics 1975;14:39.
[9] Kurtz SR. Applied Physics Letters 1985;46:1105.
[10] Fan WC, Drumm CR, Roeske SB, Scrivner GJ. IEEE Transactions on Nuclear Science 1996;43:2790.
[11] Kurtz SR, Hughes RC. Journal of Applied Physics 1983;54:229.
[12] Lenhart JL, Cole PJ, Schroeder JL, Cole SM, Belcher M, Baum N. Journal of Applied Physics 2008;103:024908.
[13] Klein RJ, Schroeder JL, Cole SM, Belcher ME, Cole PJ, Lenhart JL. Polymer 2008;49:2632.
[14] Messadi D, Vergnaud JM. Journal of Applied Polymer Science 1982;27:3945.
[15] Xu K. Chemical Reviews 2004;104:4303.
[16] Meyer WH. Advanced Materials 1998;10:439.
[17] McKean DR, Allen RD, Kasai PH, Schaedeli UP, MacDonald SA. Advances in resist technology and processing IX, vol. 1672. San Jose, CA, U S A: SPIE; 1992. p. 94–103.
[18] Vieth WR, Howell JM, Hsieh JH. Journal of Membrane Science 1976;1:177.
[19] Pandey P, Chauhan RS. Progress in Polymer Science 2001;26:853.
[20] Harogoppad SB, Aminabhavi TM. Macromolecules 1991;24:2598.
[21] Pitt CG, Jeffcoat AR, Zweidinger RA, Schindler A. Journal of Biomedical Materials Research 1979;13:497.
[22] Croll SG. Journal of Coating Technology 1986;58:41.
[23] Chrastil J. Textile Research Journal 1990;60:413.
[24] George SC, Thomas S. Progress in Polymer Science 2001;26:985.
[25] Ratner MA. In: MacCallum JR, Vincent CA, editors. Polymer electrolyte reviews, vol. 1. New York: Elsevier Applied Science; 1987.
[26] Vergnaud JM. Liquid transport processes in polymeric materials: modeling and industrial applications. New Jersey: Prentice-Hall, Inc.; 1991.
[27] McKay G, Blair HS, Gardner J. Journal of Applied Polymer Science 1983;28:1767.
[28] Mauritz KA, Storey RF, George SE. Macromolecules 1990;23:441.
[29] Smith JM, Van Ness HC, Abbott MM. Introduction to chemical engineering thermodynamics. New York: McGraw-Hill; 1996. p. 315–60.
[30] Sandler SI. Chemical and engineering thermodynamics. New York: John Wiley and Sons, Inc.; 1989. p. 305–74.
[31] Sandler SI. Chemical and engineering thermodynamics. New York: John Wiley and Sons, Inc.; 1989. p. 381–487.
[32] Weisz PB. Transactions of the Faraday Society 1967;63:1801.
[33] Weisz PB, Hicks JS. Transactions of the Faraday Society 1967;63:1807.
[34] Weisz PB, Zollinge H. Transactions of the Faraday Society 1967;63:1815.
[35] Koros WJ, Chan AH, Paul DR. Journal of Membrane Science 1977;2:165.
[36] Lardon M, Lelldoll E, Weigl JW. Molecular Crystals 1967;2:241.
[37] Melz PJ. The Journal of Chemical Physics 1972;57:1694.
[38] Hughes RC. The Journal of Chemical Physics 1973;58:2212.
[39] Woods DW. Nature 1954;174:753.
[40] Brandrup J, Immergut EH, Grulke EA, editors. Polymer handbook. 4th ed. New York: John Wiley and Sons, Inc.; 1999. p. V-114.
[41] Vrentas JS, Duda JL. Journal of Applied Polymer Science 1978;22:2325.
[42] Ponitsch M, Gotthardt P, Grüger A, Brion HG, Kirchheim R. Journal of Polymer Science, Part B: Polymer Physics 1997;35:2397.
[43] Adamson AW. Physical chemistry of surfaces. New York: John Wiley and Sons; 1976. pp. 385–94.
[44] Klein RJ, Fischer DA, Lenhart JL. Langmuir 2008;24:8187.
[45] Weast RC, editor. CRC handbook of chemistry and physics. Boca Raton: CRC Press, Inc.; 1988. p. E-53.